Materials Research Express

PAPER

Ab initio full-potential study of the fundamental properties of chalcopyrite semiconductors XPN_2 ($X = H, Cu$)

RECEIVED
4 March 2019

REVISED
16 March 2019

ACCEPTED FOR PUBLICATION
25 March 2019

PUBLISHED
5 April 2019

T Ghellab[1,2], **H Baaziz**[1,2,6], **Z Charifi**[1,2,6], **K Bouferrache**[1,2], **M A Saeed**[3] and **A Telfah**[4,5]

[1] Department of Physics, Faculty of Science, University of M'sila, 28000 M'sila, Algeria
[2] Laboratory of physics and chemistry of materials, University of M'sila Algeria
[3] Department of Physics, Division of Science and Technology, University of Education, College Road Township, Lahore, Pakistan
[4] Leibniz-Institut für Analytische Wissenschaften - ISAS - e.V. 44139 Dortmund, Germany
[5] Hamdi Mango Center for Scientific Research (HMCSR), The University of Jordan (UJ), Amman 11942 Jordan
[6] Authors to whom any correspondence should be addressed.

E-mail: baaziz_hakim@yahoo.fr **and** charifizoulikha@gmail.com

Keywords: chalcopyrite, semiconductors, optical properties, transport properties, density functional theory.

Abstract

This article reports the electronic, optical and structural properties of XPN_2 ($X = H, Cu$) chalcopyrite semiconductors by implying the density functional theory (DFT) with full potential linearized augmented plane wave plus local orbitals (APW+lo) method. The calculated electronic and structural parameters such as energy band gap, anion displacement, tetragonal ratio and lattice parameters have shown good agreement with the previous experimental and theoretical results. The optical properties are described by calculating the absorption coefficients, dielectric function along with real and imaginary part of the dielectric function. Voigt-Reuss-Hill approximations are used to calculate the set of macroscopic elastic moduli including average elastic wave velocity, Young, shear and bulk moduli, Debye temperature and Poisson's coefficient for chalcopyrite $CuPN_2$ and HPN_2. Finally, the semi-classical Bolzmann theory is applied with BolzTrap code to compute the transport properties such as thermal electrical conductivity, figure of merit and Seebeck coefficient for these materials.

1. Introduction

The crystals with the chalcopyrite structure have been extensively studied for several decades. The possible practical use of these materials as solar cells, diodes, photoelectric detectors and some other semiconductor optoelectronic devices have attracted a lot of attention. The compounds of the chalcopyrite family traditionally include the pnictides $A^{II}B^{IV}X_2^V$ (cations $A = Cd, Zn, Mg$; and $B =$ Sn, Ge, Si, and anion atoms $X =$ As, P, Sb and N) and chalcogenides $A^IB^{III}X_2^{VI}$ (anion atoms $X = O, S, Se, Te$; cations $A = Cu, Ag$; and $B = Fe, In, Ga, Al$). In contrast to the $A^{II}B^{IV}X_2^V$ group, the chemical formula of the $A^IB^VX_2^V$ (ABX_2) class of compounds involves two atoms of different types from group V of the periodic table (phosphorus and nitrogen in the case of HPN_2 and $CuPN_2$). The pnictides class $A^IB^VX_2^V$ differs considerably from $A^{II}B^{IV}X_2^V$ in displacements of composition anion from the sites of FCC lattice and degree of tetragonal compression. That is why, they are known as highly compressed chalcopyrite-like compounds. The class of $A^IB^VX_2^V$ compounds is scantly and poorly known. By now, HPN_2 [1] and $CuPN_2$ [2], have been synthesized. *X-Ray* diffraction (*XRD*) studies [1, 2] establish that these compounds are of the D_{2d}^{12} space group of symmetry and belong to the chalcopyrite family. This feature is responsible for the high ionic conductivity [3] of the ABX_2 compounds and makes these materials interesting for both experimental and theoretical studies. Ternary chalcopyrite semiconductors ($A^IB^{III}X_2^{VI}$) are used in optic-electronic devices such as non-linear optics or light emitting diodes and photovoltaic optical detectors [4–7]. They are also potential contenders for the thermoelectric applications and solar cell devices [8–13].

As the combination *P/N* of the element is isoelectronic with *Si/O*, resemblances are present with respect to properties and also in structure between the silicates and the phosphorus nitrides [14]. Analogously to silicates, an anionic vertex-sharing PN_4 tetrahedral network with three-dimensions can be produced.

The specific feature of the crystal structure of HPN_2 and $CuPN_2$ compounds is the mutual arrangement of the PN_4 tetrahedral linked to each other via vertices and the H and Cu cations located in the space between the PN_4 tetrahedral. For this reason, the authors [1, 2] consider the ideal β cristobalite (SiO_2) and chalcopyrite structures as structural and chemical analogs of the $CuPN_2$ and HPN_2 crystals. In correlating the structures of HPN_2 and $CuPN_2$ with the above-mentioned analogs, the criterion is the valence angle ϕ that describes the rotation of the tetrahedral about the tetragonal axis from zero (ideal β cristobalite) to 45° (ideal chalcopyrite). The real structure of β cristobalite can be presented as a result of $\pm 20°$ rotation of each SiO_4 tetrahedral of the ideal structure about the fourth-order axis. This yields the tetragonal symmetry with the space group D_{2d}^{12} (chalcopyrite) and two SiO_2 formula units in the unit cell [15].

Synthesis of the $CuPN_2$ semiconductor was successfully carried out from Cu_3N and P_3N_5 at a pressure of 5 GPa and 1000 °C using the Walker-type multianvil technique. From the powder x-ray diffraction data, the structure has been elucidated. The authors of reference [2] found that $CuPN_2$ is isostructural to $LiPN_2$ and $NaPN_2$ (tetragonal $I\bar{4}2d$, (n 122), a = 4.5029 (2) Å, c = 7. 0204(3)Å, V = 154.42 (1) Å^3, Rp = 1.303, wRp = 1.741) a structure derived from chalcopyrite and zinc-blende. Several semiconductors with significant features having types *IV–IV, III–V*, and *II–VI*, like *CdTe, ZnS* and *GaAs*, contain a zinc-blende type structure. Therefore, $CuPN_2$ is also supposed to have appealing electronic properties due to its structural resemblance.

Electronic bandgap measurement from experiment is hindered by the phase purity issues of $CuPN_2$ generated from the synthesis process. Even slight bits of black untraceable phosphides or phosphorus causes the reaction product having bulk samples with gray and dark colors. Therefore, band-gap of $CuPN_2$ has been calculated with DFT. They found that $CuPN_2$ is an indirect semiconductor with a band gap of 1.67 eV.

Phosphorus nitride imide HPN_2, as an inorganic polymer is one of the ternary phosphorus nitrides. Previously, it has been studied for many years [16]. Its structure is tetrahedral linked PN_4 through all four vertices with sharing corner. It has isometric analogues in the silicate family [17]. Pure and fine crystalline phosphorus imide HPN_2 is obtained by heterogeneous ammonolysis of P_3N_3 with gaseous NH_3. *X-Ray*/powder diffraction data has been used to refine the crystal structure of HPN_2 by the *Rietveld* full-profile technique. In the solid HPN_2 contains a three-dimensional framework of corner-sharing PN_4-tetrahedra. The half of the nitrogen atoms are covalently bonded with hydrogen atoms.

An inclusive study of structural, optical, thermoelectric, elastic and electronic properties of $CuPN_2$ and HPN_2 chalcopyrite semiconductors is presented by carrying out first-principles calculations within density-functional theory (DFT) using the augmented plane wave plus local orbitals (APW+lo) method. The exchange–correlation potential is treated within the local density approximation LDA [18] and the generalized gradient approximation GGA [19] for the calculation of total energy. To calculate the electronic, thermoelectric and optical properties, Engel–Vosko (EV-GGA) [20] and the modified Beck-Johnson (mBJ) functional [21] are used.

For power electronic applications, XPN_2 ($X = H, Cu$) are potential semiconductors with wide band gap. And, wide band gap semiconductor-based power devices can perform at high temperatures. Hence, the Debye temperature of XPN_2 ($X = H, Cu$) are also computed. The semi-classical *Boltzmann* theory is also used to calculate the thermoelectric properties of these semiconductors with BolzTraP code [22].

2. Computational details

Ab-initio calculations for different compounds of $CuPN_2$ and HPN_2 chalcopyrite semiconductors are done using the augmented plane wave plus local orbitals (APW+lo) method implemented in WIEN2K package [23]. It is well known fact that both local density approximation (LDA) [18] and generalized gradient approximation (GGA) [19] usually underestimate the band gap values [24, 25]. Therefore, Engel-Vosko (EV-GGA) [20] and mBJ the modified Beck-Johnson (mBJ) approaches [21] are employed to obtain more accurate band gap for the exchange and correlation effects of self-consistently. These approaches are generally more precise than the standard functional for the electronic properties of insulator and semiconductors.

The spherical harmonic expansion is used inside and plane wave basis set is chosen outside the muffin-tin sphere. Inside the atomic spheres the charge density and the potential are expanded in spherical harmonics up to $l_{\max} = 10$. An energy *cut-off* parameter $R_{MT}K_{\mathrm{MAX}}$ is discussed as $R_{MT}^{\min}K_{\mathrm{MAX}} = 8$ in order to get the total energy convergence. Self-consistent calculations are converged when the energy difference between succeeding iterations is less than 10^{-4} Ry. We have optimized the atomic positions (structural relaxation) of ternary compound XPN_2 ($X = H, Cu$), by minimization of the forces (1 mRy B^{-1}ohr^{-1}) acting on the atoms. The $R_{M.T}$ values are taken in the range 0.8–1.6 atomic units (*a.u*) for *H, Cu, P* and *N* atoms. A grid of 25 × 25 × 25k meshes was used for calculation of optical, elastic, thermoelectric properties.

Table 1. Calculated atomic positions (fractional coordinates) of $CuPN_2$ and HPN_2 with *LDA* and *GGA* approximations..

	Atomic positions		
Compounds	GGA	LDA	Experimental
$CuPN_2$	Cu: (0, 0, 0.5)	Cu: (0, 0, 0.5)	Cu: (0, 0, 0.5) [2]
	P: (0, 0, 0)	P: (0, 0, 0)	P: (0, 0, 0) [2]
	N: (0.1693, 0.25 ,0.125)	N: (0.1689, 0.25 ,0.125)	N: (0.1588, 0.25 ,0.125) [2]
HPN_2	H: (0, 0, 0.5)	H: (0, 0, 0.5)	H: (0, 0, 0.5) [3]
	P: (0, 0, 0)	P: (0, 0, 0)	P: (0, 0, 0) [3]
	N: (0.1842, 0.25, 0.125)	N: (0.1773, 0.25, 0.125)	N: (0.1462, 0.25, 0.125) [3]

3. Results and discussions

3.1. Structural properties

The *x-ray* diffraction is used to get the structural parameters of $CuPN_2$ and HPN_2 [1, 2]. The space group of these compounds is found to be D_{2d}^{12} (is structural analogs of chalcopyrite).

In this study the compounds are relaxed completely for all volumes using the optimization of the force. The atomic positions for each compound are calculated with LDA and GGA approximations. Table 1 shows the comparison of atomic positions with experimentally available data and they are in good agreement with the experimental findings [2, 3].

$CuPN_2$ and HPN_2 are crystallizing with space group $I\bar{4}2d$(n 122) composed of cristobalite-type P/N network which is isostructural to $LiPN_2$ and $NaPN_2$ [26, 27]. Each PN_4 tetrahedron is linked with four neighboring PN_4 tetrahedral by shared corners (see figure 1). *Cu* (*H*) is also coordinated in a distorted-tetrahedral manner by four N atoms. Due to the covalent nature of *P-N* and *Cu (H)-N* bonds, the $CuPN_2$ (HPN_2) can be treated as a double nitride. Whereas, the PN_4 tetrahedral with angles (from 109.73° to 108.96°) are close to regular tetrahedral and *P-N* distance of 1.6385 (1.599) Å, the CuN_4 (HN_4) tetrahedral are considerably more deformed and flattened along *c*. These leads to $\theta_{(P\text{-}N\text{-}P)}$ of $CuPN_2$ (HPN_2) angle that derivate markedly from a regular tetrahedron angle with values ranging between 125.41° (123.08°) to 125.74° (121.12°) using GGA and LDA respectively (see table 2). The *Cu-N* and *P-N* distances are reasonable with the sum of the ionic radius (2.09 Å and 1.63 Å respectively) according to [28].

The crystal structure of XPN_2 ($X = H, Cu$) can be regarded as a transition between chalcopyrite/zinc-blende and cristobalite. Taking ideally filled β-cristobalite as an initial, a rotation of the tetrahedral by a rotation angle of 45° about the $\bar{4}$ axis leads to tetrahedral arrangement found in regular chalcopyrite [26, 29]. The bonding angle changes from 180° (β-cristobalite) to 109.5 (chalcopyrite). Thus, according to the bonding angle *P-N-P* and rotation angle φ, the structures of XPN_2 ($X = H, Li, Na, Cu$) can be positioned between chalcopyrite and β-cristobalite; table 2. The values obtained for $CuPN_2$ lie between $LiPN_2$ and $NaPN_2$ placing $CuPN_2$ nearer to β-cristobalite than $LiPN_2$ but nearer to the chalcopyrite structure than $NaPN_2$ [26, 27].

As well know, the chalcopyrite structure is described by three parameters two lattice constants *a* and *c*, and internal parameter *u*, which define the position of anions in the base plane of unit cell (*xy* plane). The atomic coordinates and lattice parameters of nitrogen using GGA are (0.1693, 0.25, 0.125) and $a = 4.5509$ Å, $c = 7.7422$ Å, for $CuPN_2$; and are (0.1842, 0.25, 0.125) and $a = 4.6556$ Å, $c = 7.8221$ Å for HPN_2. Table 2 shows the theoretical structural parameters agreement with experimental data. From the results in table 2, it can be noted that the deviation of the lattice parameters from the experiment is smaller in the case of LDA than the GGA calculations. The LDA approximation is therefore a good choice for studying the structural properties of $CuPN_2$ and HPN_2 compounds. The *u* parameters for XPN_2 ($X = H, Cu$) compound as $u = \frac{1}{4} + \frac{(d_{X-N}^2 - d_{P-N}^2)}{a^2}$ where d_{X-N} and d_{P-N} are the bond lengths among the corresponding atoms. An ideal chalcopyrite lattice has $u = 1/4$ and $c/a = 2$. The real compounds of chalcogenide $A^I B^{III} X_2^{VI}$ and pnictides $A^{II} B^{IV} X_2^V$ groups have $u = 0.214$–0.304 and $c/a = 1.769$–2.016 in most cases [30]. The structural parameter values of XPN_2 ($X = H, Li, Na, Cu$) are going far beyond these boundaries.

From table 2, the experimental and theoretical *u* values have interval (0.32–0.34), while the c/a ratio have interval (1.68–1.72) characterizing tetragonal distortion. Thus XPN_2 ($X = H, Cu$) compound can be revealed as a discrete group of extremely compressed chalcopyrite compounds.

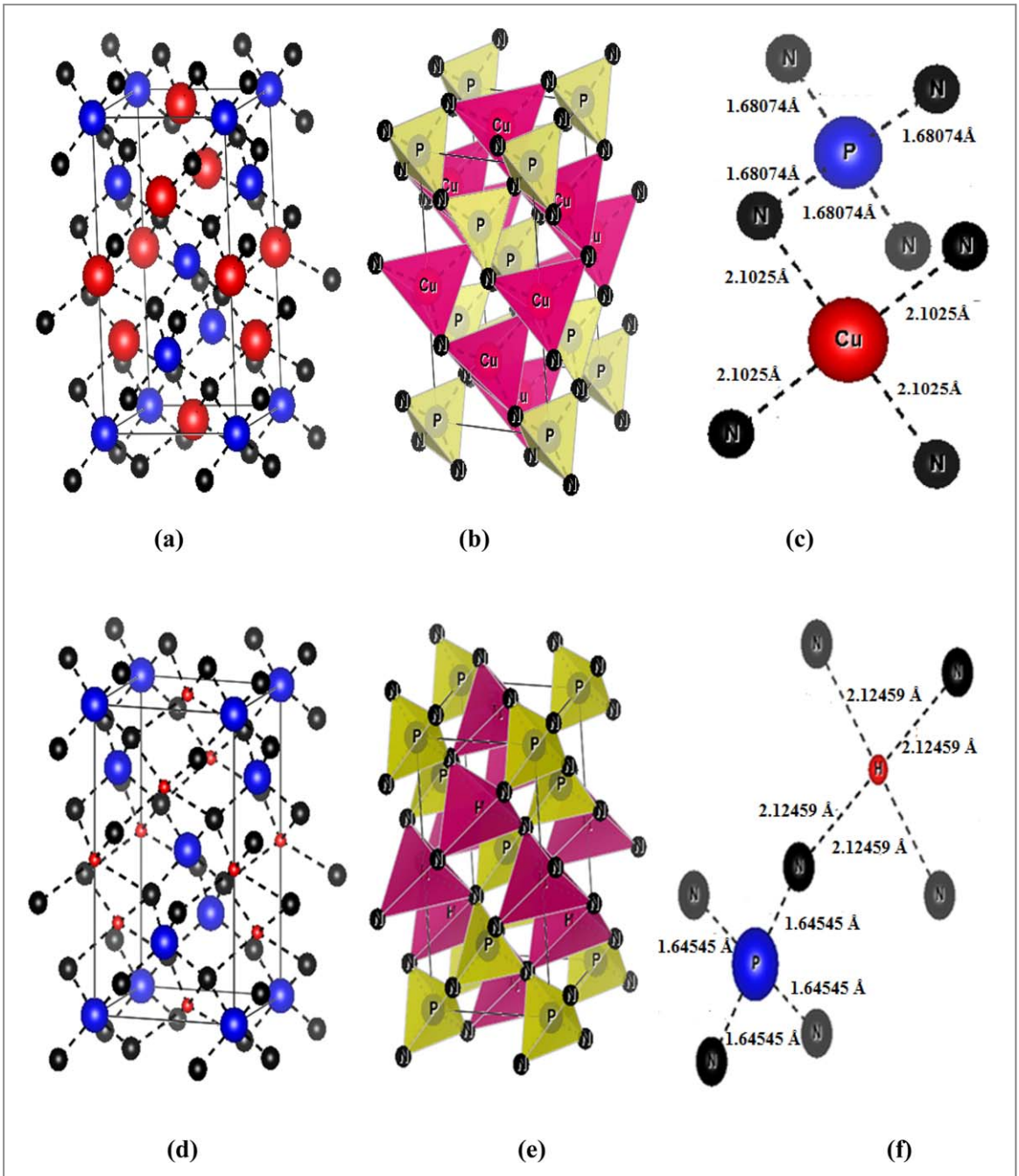

Figure 1. Crystal structure of XPN_2 ($X = Cu, H$): (a) and (d) Tetragonal centered ($I\bar{4}2d$ space group) of $CuPN_2$ and HPN_2 respectively according to the plan (111), (b) and (e) Tetrahedral configuration of groups in $CuPN_2$ and HPN_2, (c) and (f) Projection in (110) and (101) of $CuPN_2$ and HPN_2 respectively. Black: *N*; Blue: *P*; Red: *Cu, H*.

The structural parameters of XPN_2 ($X = H, Cu$) have substantial differences which are related to different size of the atoms. The theoretical data suggest that the replacement of *H* atoms with larger *Cu* atom decreases bond length very weakly between nitrogen atoms and these atoms by 0.95%; while the bond length of *P-N* increases by 2.38% (2.42%) occurs with GGA (LDA).

3.2. Electronic band structure and density of states (DOS)

The scalar relativistic self-consistent band structures of HPN_2 and $CuPN_2$ compounds along representative symmetrical directions of the *Brillouin* zone were obtained at both equilibrium and far from equilibrium volume within the GGA, LDA, mBJ-GGA, mBJ-LDA approximations. A dashed horizontal line is used to illustrate the Fermi level E_f.

Figure 2 shows the band structure of $CuPN_2$ and HPN_2 compounds. The graphs show the gap between the conduction and valence bands calculated within mBJ-LDA approximation are 2.647 eV and 2.191 eV for HPN_2

Table 2. Theoretical and experimental structural parameters and interatomic distances (in Å) and angles within PN_4 using the *LDA* and *GGA* of $CuPN_2$ and HPN_2.

Compounds	Approximations		Experimental
	GGA	LDA	
$CuPN_2$	$a = 4.5509$	$a = 4.4728$	$a = 4.5029$ [2]
	$c = 7.7422$	$c = 7.6991$	$c = 7.6156$ [2]
	$c/a = 1.7013$	$c/a = 1.7212$	
	$d_{Cu\text{-}N} = 2.1025$ Å	$d_{Cu\text{-}N} = 2.0901$	$d_{Cu\text{-}N} = 2.1294$ [2]
	$d_{P\text{-}N} = 1.6807$	$d_{P\text{-}N} = 1.6577$	$d_{P\text{-}N} = 1.6385$ [2]
	$u = 0.3270$	$u = 0.3310$	
	$B_0 = 224.44$	$B_0 = 243.70$	
	$B' = 5.23$	$B' = 3.53$	
	$\Delta a/a = +1.05$	$\Delta a/a = -0.67$	
	$\Delta c/c = +1.63$	$\Delta c/c = +1.08$	
	$\varphi = 34.10°$	$\varphi = 34.04$	$\varphi = 32.4°$ [2]
	$\theta_{(P\text{-}N\text{-}P)} = 125.41°$	$\theta_{(P\text{-}N\text{-}P)} = 125.74°$	$\theta_{(P\text{-}N\text{-}P)} = 128.3°$ [2]
HPN_2	$a = 4.6556$	$a = 4.5491$	$a = 4.6182$ [3]
	$c = 7.8221$	$c = 7.2141$	$c = 7.0204$ [3]
	$c/a = 1.6801$	$c/a = 1.6901$	
	$d_{H\text{-}N} = 2.1245$	$d_{H\text{-}N} = 2.1132$	$d_{P\text{-}N} = 1.599$ [3]
	$d_{P\text{-}N} = 1.6454$	$d_{P\text{-}N} = 1.6119$	
	$u = 0.3333$	$u = 0.3402$	
	$B_0 = 101.52$	$B_0 = 117.59$	
	$B' = 4.68$	$B' = 4.78$	
	$\Delta a/a = +0.8$	$\Delta a/a = 0.43$	
	$\Delta c/c = +10.2$	$\Delta c/c = +9.66$	
	$\varphi = 36.38°$	$\varphi = 35.31°$	$\varphi = 36.38°$
	$\theta_{(P\text{-}N\text{-}P)} = 123.08°$	$\theta_{(P\text{-}N\text{-}P)} = 121.12°$	

$\varphi = -\tan^{-1}(4x)$ with $x = x$ coordinate of N, strictly valid only for regular PX_4 tetrahedra. φ (β-Cristobalite) = 0°, φ (Chalcopyrite) = 45°, θ (β-Cristobalite) = 180°, θ (Chalcopyrite) = 109.5°

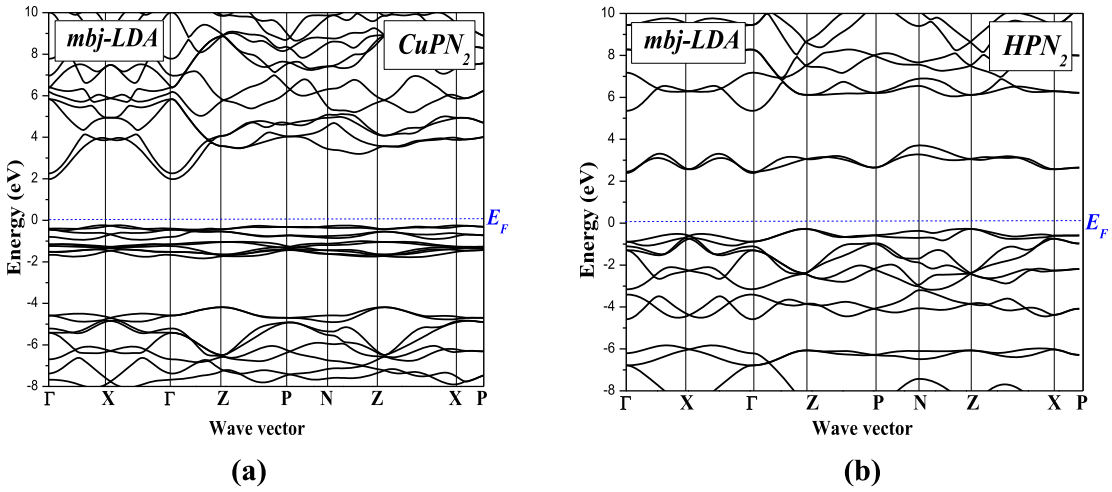

Figure 2. Band structure along the symmetry lines of the *Brillouin* zone for (a) $CuPN_2$ (Centered tetragonal; $I\bar{4}2d$) compound, (b) HPN_2 (Centered tetragonal; $I\bar{4}2d$) compound. The position of the *Fermi* level is shown by the horizontal line.

and $CuPN_2$ respectively which gives HPN_2 and $CuPN_2$ the property to become a large band-gap semiconductor material. It has observed that the band dispersions in HPN_2 and $CuPN_2$ are very similar.

The HPN_2 having a gap in the Z-Γ direction makes it an indirect band gap material, while in $CuPN_2$, the maximum and minimum of valence band are found at the X-Γ direction and Γ point respectively and leads an indirect band gap. The respective calculated values of the band gaps are listed in table 3.

In figure 3, a graph is plotted between the mainly contributing element and complete *DOS* for each compound below the *Fermi* energy (E_F). The corresponding band structures and k-path Γ-X-Z-P-N of two compounds is shown in figure 2. The *DOS* clearly shows that in HPN_2 the area below E_F, is dominated by

Table 3. The energy gap *Eg* calculated in the approximations *LDA*, *GGA*, *EV-GGA* and *mBJ* of $CuPN_2$ and HPN_2.

	Our calculation					Other calculationsDFT [2]			
Compounds	*GGA*	*LDA*	*EVGGA*	*mBJ-LDA*	*mBJGGA*	$CuPN_2$	$MgSiP_2$	$LiPN_2$	$NaPN_2$
$CuPN_2$	1.571	1.791	1.387	2.191	2.135	1.67	1.33	3.84	4.66
HPN_2	1.681	1.963	1.942	2.647	2.400				

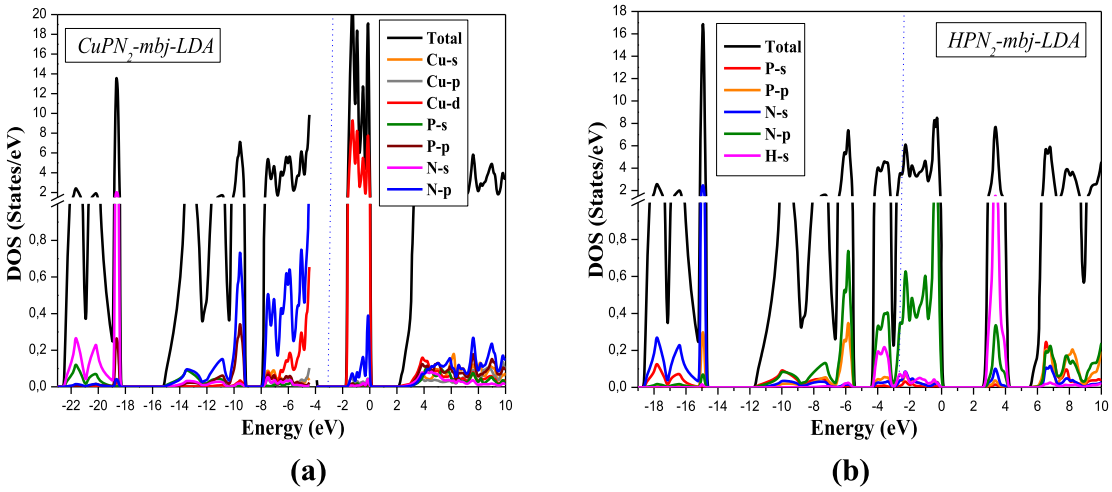

Figure 3. The calculated total and partial density of states for $CuPN_2$ and HPN_2 compounds. The graph is scaled for 0 eV at the *Fermi* level (E_F).

nitrogen states, while in $CuPN_2$ the states of copper are superior. The *Cu-d* states contribution lead to reduction in band gap as compared to HPN_2. Three allowed energy bands make the valence band of HPN_2 and $CuPN_2$, which is in qualitative agreement with the valence band structure of the $A^{II}B^{IV}X_2^V$ compounds with a chalcopyrite lattice [31]. However, the atomic composition and strong tetragonal compression among the HPN_2 and $CuPN_2$ crystals causes valence bands of these compounds to become different. The structures of the valence band of $CuPN_2$ and HPN_2 crystals are qualitatively similar, since the bands basically originate from the sp^3 states of *P* and *N* atoms. By analogy with the $A^{II}B^{IV}X_2^V$ compound, the lower set of valence bands in HPN_2 and $CuPN_2$ is formed predominantly from the phosphorus and nitrogen states in a ratio of 1:3 having a small contribution (14%) from the *p* states of phosphorus.

The next set has a major contribution from the nitrogen *p* states and a minor contribution from the *p* states of phosphorus. This is untypical of the ABX_2 compounds of the chalcopyrite family, in which this band is formed basically of the *s* states of the cation *B*. The *p* states contribution of phosphorus balance nearly half of the nitrogen atom's *p* states. Therefore, the valence band's lower sets of $CuPN_2$ and HPN_2 are qualitatively considered to be identical in the dominant contribution from the *s* and *p* states of phosphorus or nitrogen. $A^IB^{III}X_2^{VI}$ and $A^{II}B^{IV}X_2^V$ pnictides differ substantially even though they are similar qualitatively in their valence bands. The $A^{II}B^{IV}X_2^V$ having chalcopyrite structure, while the second set generally contains two levels of energy. It consists of three levels in HPN_2 and $CuPN_2$ and the topology of the second set is repeated completely.

Furthermore, for $A^IB^{III}X_2^{VI}$, the *p* states of the nitrogen usually form the upper set and it contain not only the *p* states of nitrogen but also a significant addition of the *p* states of phosphorus. The mechanism of donor-acceptor bond formation in HPN_2 and $CuPN_2$ determines this partial composition, with the leading contribution from the donor nitrogen and accepter phosphorus atoms. The stable PN_4 tetrahedral is formed from the empty *p* orbitals of phosphorus. A vacant '*s*' orbital is formed by the loss of valence electron of *H* and (*Cu*) ions in the crystal, which is more energetically favorable for H^+ than Cu^{+2}, to precise a lone pair electron of nitrogen. This describes the more bond stability in $CuPN_2$ than in HPN_2.

Another characteristic of HPN_2 and $CuPN_2$ is a significant band widening in the valence band of the allows energy levels as compared with the bands of $A^{II}B^{IV}X_2^V$ with a chalcopyrite lattice and it is described by the increased degree of *s*, *p*, *d*-hybridization of the atomic states which are responsible for the establishment of the corresponding crystal orbitals.

The total width of the valence band of the XPN_2 ($X = H, Cu$) compounds is ~20 eV, nearly 1.5 times larger than the typical widths for the chalcopyrite family. This is due to the *N* atoms entering into the composition of these compounds.

3.3. Optical properties

As a potential candidate for the optoelectronic applications, the study of the optical properties of XPN_2 ($X = H$, Cu) chalcopyrite semiconductors is very crucial. It is understood that there is a direct relationship between the main optical parameters of materials and their complex dielectric function, $\varepsilon(\omega) = \varepsilon_1(\omega) + i\varepsilon_2(\omega)$, where $\varepsilon_1(\omega)$ is the real part and $\varepsilon_2(\omega)$ is the imaginary part of the dielectric function. The following equations are used to calculate the imaginary and real part of the dielectric function [32].

$$\varepsilon_2(\omega) = \frac{8}{3\pi\omega^2}\sum_{nn'}\int_{BZ}|P_{nn'}(k)|^2\frac{dS_k}{|\nabla_k\omega_{nn'}(k)|} \tag{1}$$

Rydberg atomic units are used to write the above expression with $e^2 = 1/m = 2$ and $\hbar = 1$.

The photon energy is given by $\omega_{nn'}(k)$. $P_{nn'}(k)$ is the dipolar matrix element and the energy difference is given by $\omega_{nn'}(k)$. $\omega_{nn'}(k) = E_n(k) - E_{n'}(k)$ and S_k is a constant energy surface $S_k = \{k;\omega_{nn'}(k) = \omega\}$.

In the case of polarizability, $\alpha = \alpha_1 + i\alpha_2$, these conditions are respected. We then have Kramers-Kronig relations [33].

$$\alpha_1(\omega) = \frac{2}{\pi}P\int_0^{+\infty}\frac{\omega'\alpha_2(\omega')}{\omega'^2 - \omega^2}d\omega' \tag{2}$$

$$\alpha_2(\omega) = -\frac{2\omega}{\pi}P\int_0^{+\infty}\frac{\omega'\alpha_1(\omega')}{\omega'^2 - \omega^2}d\omega' \tag{3}$$

Where ω is the frequency and P is the main part of the Cauchy integral, defined by

$$P = \lim_{\alpha\to 0}\int_{-\infty}^{\omega-a}\frac{\alpha(\omega')}{\omega' - \omega}d\omega' + \int_{\omega+a}^{+\infty}\frac{\alpha(\omega')}{\omega' - \omega}d\omega' \tag{4}$$

Kramers–Kronig expressions are used to estimate the real part $\varepsilon_1(\omega)$ from $\varepsilon_2(\omega)$ [33].

$$\varepsilon_1(\omega) = \mathrm{Re}\,\varepsilon(\omega) = 1 + \frac{2}{\pi}P\int_0^{+\infty}\frac{\omega'\varepsilon_2(\omega')}{\omega'^2 - \omega^2}d\omega' \tag{5}$$

In the crystal the reflectivity, absorption coefficient, refractive index and extinction coefficient given by $R(\omega)$, $I(\omega)$, $n(\omega)$ and $k(\omega)$ respectively, are related to the reflectivity by [34]

$$R(\omega) = \frac{n + ik - 1}{n + ik + 1} \tag{6}$$

$$I(\omega) = \sqrt{2}\,\omega[\sqrt{\varepsilon_1(\omega)^2 + \varepsilon_2(\omega)^2} - \varepsilon_1(\omega)]^{1/2} \tag{7}$$

$$k(\omega) = I(\omega)/2\omega \tag{8}$$

$$n(\omega) = (1/\sqrt{2})[\sqrt{\varepsilon_1(\omega)^2 + \varepsilon_2(\omega)^2} + \varepsilon_1(\omega)]^{1/2} \tag{9}$$

The dielectric functions comprise of two components $\varepsilon_{xx}(\omega)$ and $\varepsilon_{zz}(\omega)$. $\varepsilon_{xx}(\omega)$ is related to the polarization along the x and y directions ($E\perp c - axis$), while $\varepsilon_{zz}(\omega)$ is corresponding to the z direction ($E\|c - axis$).

The calculation results of the imaginary part of the dielectric function in the energy range from 0 to 40 eV for HPN_2 and $CuPN_2$ compounds are illustrated in figure 4. From this curve, which reflects the absorption of the material, we can obtain the different interband transitions.

The analysis of these spectra shows that the behavior of $\varepsilon_2(\omega)$ is almost similar for all, and the first critical points of the dielectric function that corresponds to the fundamental absorption thresholds start at about 2.1905, and 2.6259 eV for $CuPN_2$, HPN_2, respectively. The origin of these points is due to the optical transition between the highest valence band and the lowest conduction band, then the values of the critical points correspond to the transition (X-$\Gamma \rightarrow \Gamma$) and (Z-$\Gamma$) respectively. Thus, we notice next to the fundamental peak the main peaks that reflect the maximum absorption, are located at 8.96 and 3.66 eV for $CuPN_2$, HPN_2 respectively. So, the imaginary part of dielectric function shows a main peak in the *Ultra-violet* region for all compounds. For all compounds, the imaginary part of dielectric function rapidly decreases after this peak.

The evolution of the extinction coefficient as a function of the energy of the compounds studied is shown in figure 4. The spectra are similar with small differences in detail. The maximum value of the extinction coefficient observed on the spectra and corresponding to the energies 11.19, 3.82 eV for $CuPN_2$, HPN_2 compounds respectively corresponds to the zero of $\varepsilon_1(\omega)$. The energy where the extinction coefficient reaches its maximum value is that where the real part of the dielectric function is zero.

The dielectric function's real part is attained from the imaginary part with the help of Kramers-Kronig transformations [35], presented in figure 5. Static dielectric constants from the zero-frequency limit are calculated; table 4.

It is noted that these optical spectra shown in this figure are similar with small differences (the position and the height of the peaks). Figure 5 shows the calculated results of the real (dispersive) part $\varepsilon_1(\omega)$ of the dielectric function of the compounds XPN_2 ($X = H$, Cu). The zero crossing of spectra means the non-existence of

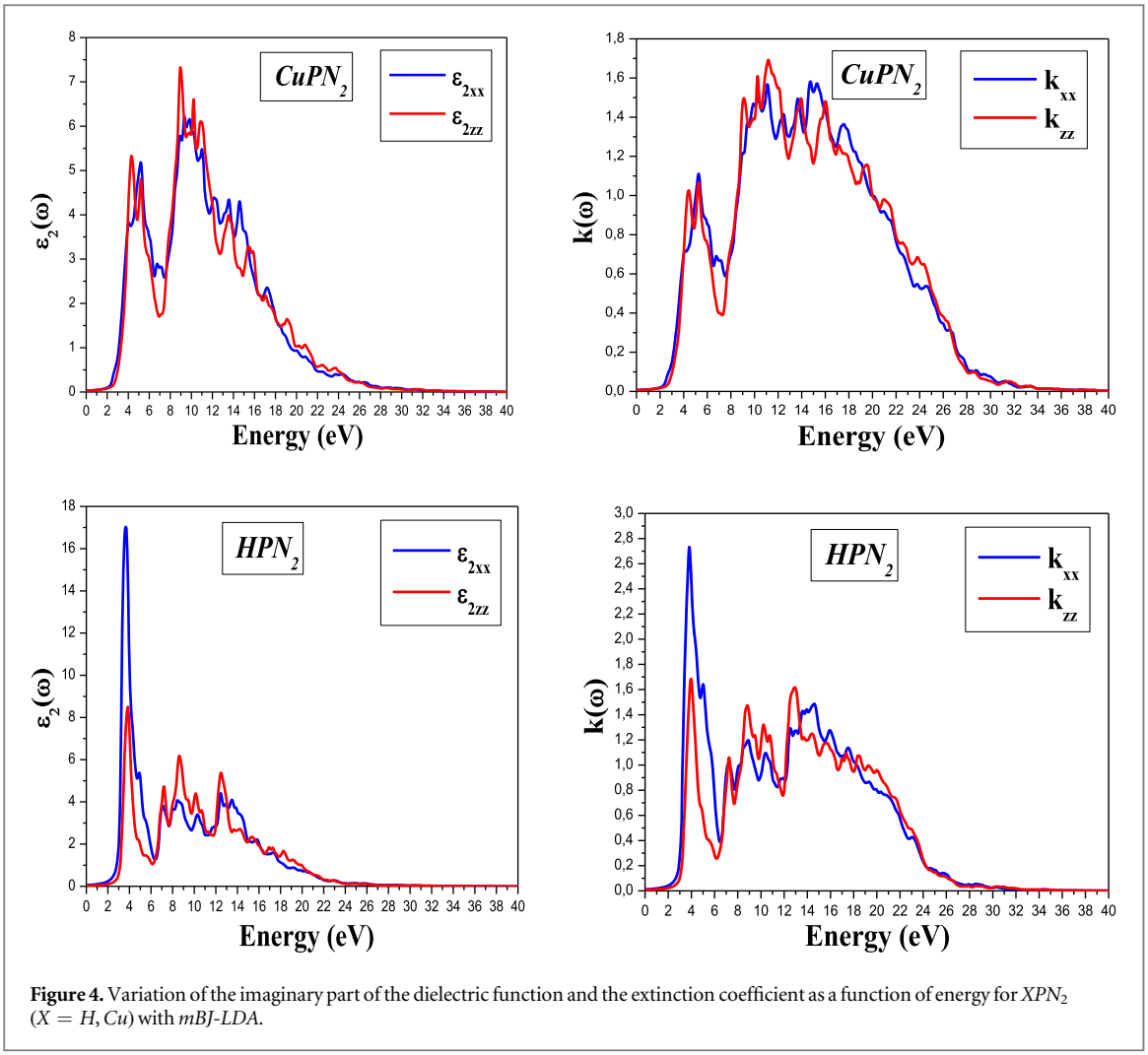

Figure 4. Variation of the imaginary part of the dielectric function and the extinction coefficient as a function of energy for XPN_2 ($X = H, Cu$) with *mBJ-LDA*.

diffusion. We have noticed that for all these compounds, the function $\varepsilon_1(\omega)$ becomes zero, where the dispersion at these energy values is zero and consequently the absorption is maximal.

Figure 5 shows that from the values $\varepsilon_1(0)$, the real part increases with the increase of photon energy, reaches the major peaks and becomes zero. After passing through a minimum, the dispersive part $\varepsilon_1(\omega)$ again reaches the zero.

The main peaks of $\varepsilon_1(\omega)$ obtained from mBJ-LDA calculations are situated at 3.63 eV, 3.24 eV for $CuPN_2$ and HPN_2 compounds, respectively. These are located in the *Ultra-Violet* spectrum. The real part of the dielectric function becomes zero at energies 11.15 eV, 3.67 eV for $CuPN_2$ and HPN_2 respectively. The principal peak is followed by an oscillating structure around zero, then the spectrum becomes negative, a minimum followed by a slow progression towards zero around 26.89 eV for $CuPN_2$ and HPN_2 at about 24.06 eV. The peak with the highest intensity is observed for HPN_2.

The real part of the dielectric function in a low energy region is negative which is mainly due to a greater value of extinction coefficient $k(\omega)$ than the refractive index $n(\omega)$ [34] and these values correspond to the maximum reflection of incident photons in these regions. The large negative value of ε_1 at low energies is because of the free electron mechanism and the positive value of ε_1 is generally related to interband transitions of bonding electrons [36].

From figure 5, we can see a slight anisotropy for the two compounds $CuPN_2$ and HPN_2 in the real part of the dielectric function near the main peak. In addition, $CuPN_2$ shows a higher dielectric constant than HPN_2.Penn model has explained this effect, $\varepsilon_1(0) \approx 1 + \left(\frac{\hbar\omega_P}{E_g}\right)^2$ [37] where E_g and ω_P are the energy band gap and the plasma frequency respectively, the band gap of HPN_2 is greater than that of the $CuPN_2$ compound. This means that a small energy gap gives a great value of $\varepsilon_1(0)$.

Optical properties such as reflectivity spectra $R(\omega)$ and absorption coefficient $I(\omega)$ can be estimated from the real and imaginary parts attained from the frequency-dependent dielectric function.

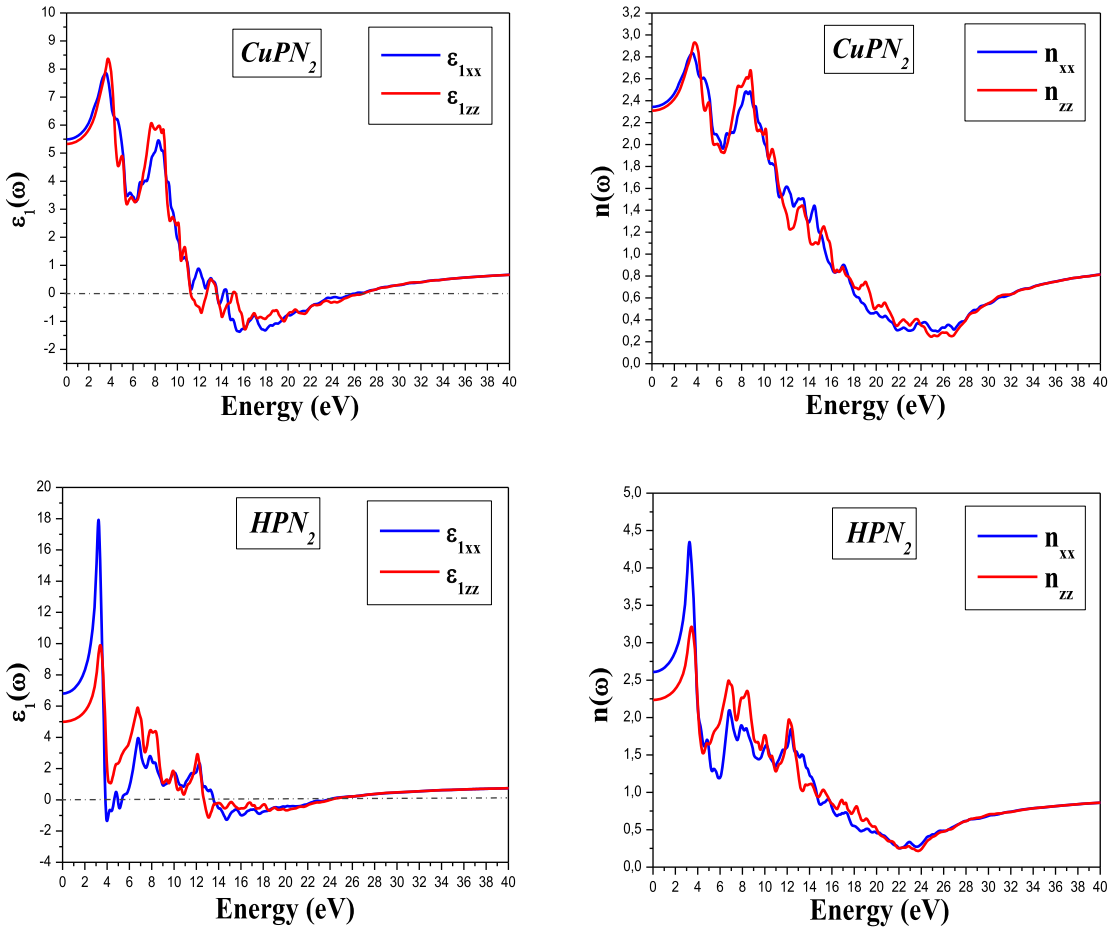

Figure 5. Variation of the real part of the dielectric function and the refractive index as a function of energy for XPN_2 ($X = H, Cu$) with *mBJ-LDA*.

The refractive index determines the amount of reflected light after reaching the interface. In optical devices, for total internal reflection, it also determines the critical angle. These optical properties enhance its importance in many applications. The spectra are shown in figure 5 where the refractive index generally follows the shape of the real part to which it is bound by $n(0) = \sqrt{\varepsilon_1(0)}$. In refractive index spectrum, the excitonic transitions cause the sharp peaks at the energy band gap edge.

The zero-frequency refractive indexes of the compounds are 2.42, 2.32 for HPN_2, $CuPN_2$ respectively. The refractive index value decreases with the increase in frequency up to 10 eV and after that it started to increase up to 25 eV and also show a nonlinear behavior.

The calculated static refractive index $n(0)$ is summarized in the same table with $\varepsilon_1(0)$. To the best of our knowledge, no experimental data is available for comparison. The calculated results also show that the real part $\varepsilon_1(\omega)$ and the refractive index $n(\omega)$ are slight anisotropic.

The reflectivity spectrum is presented in figure 6, it is observed that at low energies these chalcopyrite semiconductors have a small reflectivity. It's starting from 15% and 20% for $CuPN_2$ and HPN_2 respectively, and then at high and intermediate energies, a prompt increase in reflection occurs. The maximum reflectivity occurs at 21.79 eV for $CuPN_2$, 3 and 21.79 eV. These reflectivity maxima result from interband transitions.

The absorption coefficient $I(\omega)$ is another crucial optical constant which gives the measure of the light absorbed by a given medium. Figure 6 shows the absorption coefficients of XPN_2 ($X = H, Cu$). It was noted that the absorption coefficient increases in low energies considerably to reach its maximum value at higher energies. The absorption coefficient $I(\omega)$ is greater (10^4 cm^{-1}) and increases rapidly.

For $CuPN_2$ (HPN_2), I_{xx} is highest and occurs at 15.31 (14.65) eV with absorption spectra indicating maximums in the energy range 9.29–24.88 (12.13–22.02) eV. So, in the *Ultra-Violet* region for all compounds, the highest absorption peaks occur. The interband transitions in electronic band spectrum between various high symmetries are responsible for the production of these peaks. In figure 6, the mBJ-LDA results show that the main peaks for I_{xx} are higher than the I_{zz} results for the two semiconductors and it means that the absorption along the x and y ($E \perp c$) axis is higher than the z direction ($E \| c$) axis. It is observed that these compounds may be good absorber of medium and low *Ultra-violet* spectrum as presented in figure 6.

Table 4. $\varepsilon_1(0)$ calculated and $n(0)$ of compounds $CuPN_2$ and HPN_2 in *LDA*, *GGA*, *EV-GGA* and *mBJ*.

Compounds	$\varepsilon_1(0)$						$n(0)$					
		GGA	*LDA*	*EVGGA*	*mBJ GGA*	*mBJ LDA*		*GGA*	*LDA*	*EVGGA*	*mBJ GGA*	*mBJ LDA*
$CuPN_2$	ε_{1xx}	9.7560	6.8188	11.2714	5.5920	5.4914	n_{xx}	3.1235	2.61131	3.3573	2.36477	2.34339
	ε_{1zz}	6.5950	6.6230	7.04795	5.4075	5.3303	n_{zz}	2.5681	2.57354	2.6548	2.32542	2.30876
HPN_2	ε_{1xx}	6.4585	9.4133	6.11869	6.9081	6.8061	n_{xx}	2.5413	3.06816	2.47361	2.62836	2.60889
	ε_{1zz}	6.2091	6.6068	5.92921	5.1421	4.9974	n_{zz}	2.4918	2.57041	2.43501	2.26765	2.23552

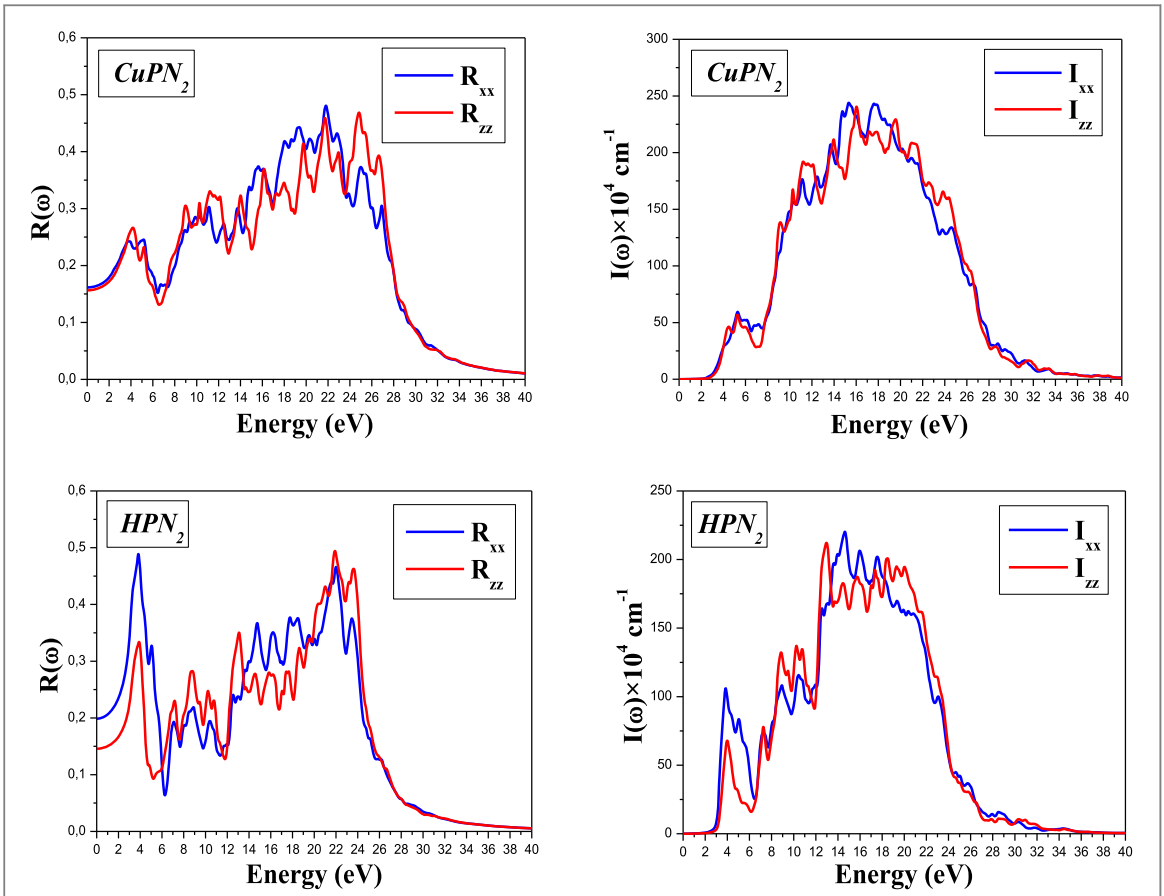

Figure 6. Variation of the reflectivity and the absorption coefficient as a function of energy for XPN_2 ($X = H, Cu$) with *mBJ-LDA*.

At low energies (~12 eV), the transitions between very close lying energy levels causes the broadening in the absorption spectrum. However, for HPN_2 a sharp peak at 3.6 eV is observed and can be related to the sharp transitions that occur between the well separated conduction and valence bands.

The optical conductivity $\sigma(\omega)$ relates the oscillating electric field $E(\omega)$ with current density $j(\omega)$ as follows [38]:

$$j(\omega) = E(\omega)\sigma(\omega) \tag{10}$$

And when $\omega \rightarrow 0$, it converts to electrical conductivity. It has a direct relation to the imaginary part of the dielectric function, and its real part can be calculated by the following relation [39]:

$$\sigma(\omega) = \frac{\omega}{4\pi}\varepsilon_2 \tag{11}$$

Several peaks corresponding to interband transitions are present in the optical conductivity spectrum shown in figure 7. Sharp edges occur at 8–16 eV in the *ultraviolet* region.

The energy loss function is an essential factor depicting the energy loss of fast-moving electrons in the material. The energy loss function can be calculated from the dielectric function. It can be described by the expression:

$$L(\omega) = \mathrm{Im}\left(-\frac{1}{\varepsilon(\omega)}\right) \tag{12}$$

This can also be written as follows

$$L(\omega) = \left(\frac{\varepsilon_2(\omega)}{\varepsilon_1(\omega)^2 + \varepsilon_2(\omega)^2}\right) \tag{13}$$

As shown in figure 7, the energy loss spectra show significant values in the energy region between 25.70 and 27.86 eV for $CuPN_2$. The intense peak is observed at energy of 27.05 eV.

Regarding HPN_2, its energy range 23.46–24.53 eV is characterized by a significant loss of energy. The peak along the *z*-axis is highest at 24.09 eV for HPN_2.

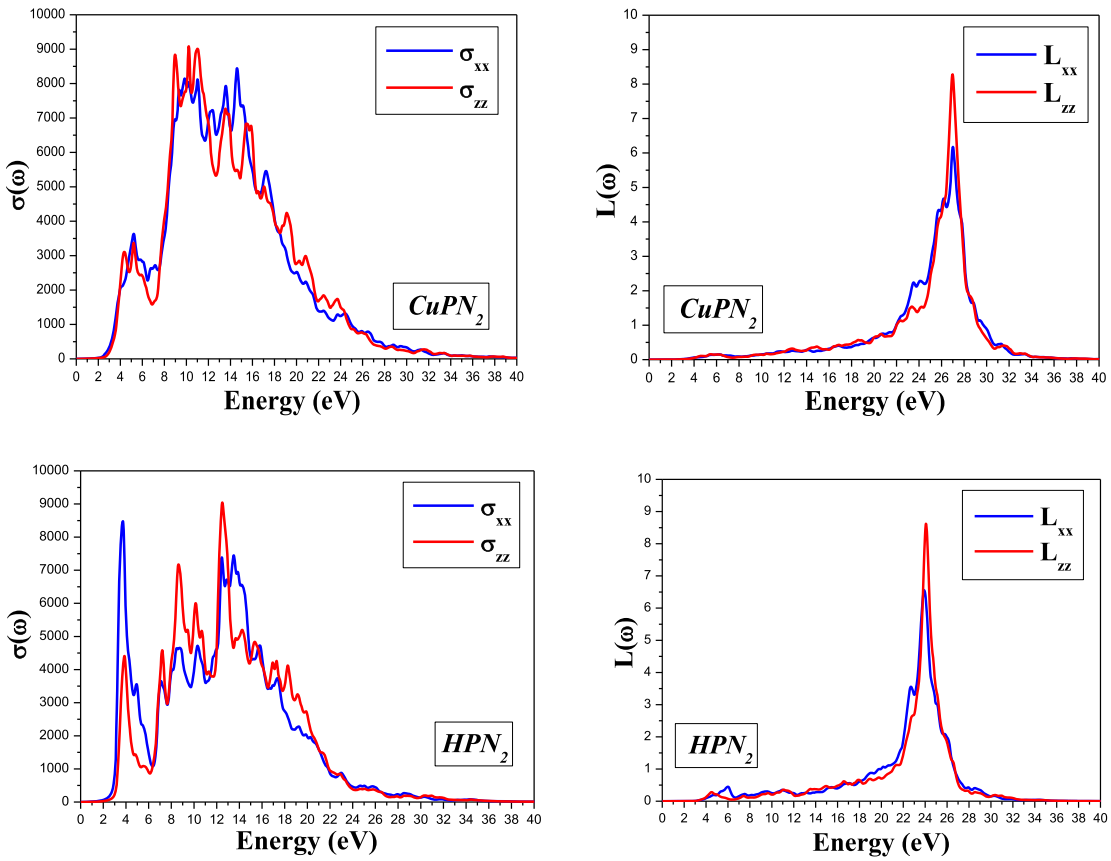

Figure 7. Variation of the optical conductivity and the energy loss function as a function of energy for XPN_2 ($X = H, Cu$) with *mBJ-LDA*.

Note that for XPN_2 ($X = H, Cu$) chalcopyrite semiconductors, the major peak occurs when $\varepsilon_2(\omega)$ is very small and $\varepsilon_1(\omega)$ reaches zero again. The plasma frequency ω_p is the mean peak of the energy loss function. Therefore, by way of example, the plasma energy $\hbar\omega_p$ of its peak position is 27.05 eV, 24.09 eV for $CuPN_2$ and HPN_2 respectively.

3.4. Elastic properties

The physical properties of solids can be understood with the information of the elastic constants. In particular, elastic constants determine the elasticity and mechanical stability of crystals. In single-crystal state, the elastic properties of tetragonal systems can be completely characterized with the following six independent elastic constants, named as C_{11}, C_{33}, C_{44}, C_{66}, C_{12} and C_{13}. The computed elastic constants of the XPN_2 ($X = H, Cu$) chalcopyrite semiconductors are given in table 5. In the case of HPN_2 and $CuPN_2$, to the best of our knowledge, there is no theoretical or experimental data is available in the literature for these constants to compare with our results.

The obtained results (table 5) show that the values of the constants (C_{11} and C_{33}) representing the crystal's resistance to compression along its [100] and [001] principle crystallographic directions, respectively, are higher than those of C_{44}, C_{66}, C_{12} and C_{13} constants, which stand for the crystal's resistance to shear. In all investigated systems, the C_{11} is larger than C_{33} indicating the hardness of the XPN_2 ($X = H, Cu$) chalcopyrite semiconductors along the *a*- and *b*-axes (i.e. [100]/[010]) is higher than that along the *c*-axes (i.e. [001]). The possible reason is the high stiffness of the *P-N* bond which lies along the [100] and [010] directions (see figure 1). The C_{11} of $CuPN_2$ is higher than that of HPN_2, this can be explained by the more strength of *Cu-N* bond in $CuPN_2$ compared to the corresponding one *H-N* in HPN_2 (see section 3.1). It can be noted from table 5 that C_{33} value in HPN_2 is smaller than the corresponding one in $CuPN_2$. This can be associated to the more strength of the *Cu-N* bond in $CuPN_2$ compared to the corresponding one *H-N* in HPN_2 (see table 2). Thus, we can conclude that $CuPN_2$ stiffest across *a*-axis and *c*-axis than the HPN_2.

The elastic constant C_{44} is interrelated to the monoclinic shear distortion along the [010] direction in the (100) plane and the C_{66} is related to the resistance to shear along the [110] direction in the (100) plane. In the four materials, the value of C_{44} is greater than that of C_{66}. The C_{44}/C_{66} ratio, also called shear anisotropy ratio (A), is

Table 5. The elastic constants for $CuPN_2$ and HPN_2 calculated using *GGA* and *LDA* approximation.

Compounds	$CuPN_2$		HPN_2	
Approximations	GGA	LDA	GGA	LDA
$\mathbf{C_{11}}$	354.6031	376.1744	256.343	237.185
$\mathbf{C_{12}}$	131.7750	162.1137	29.436	32.317
$\mathbf{C_{13}}$	181.7375	189.9158	60.218	74.301
$\mathbf{C_{33}}$	331.7116	337.7635	171.429	190.353
$\mathbf{C_{44}}$	206.2482	231.7541	109.492	126.248
$\mathbf{C_{66}}$	174.0155	196.1452	38.300	61.161
$\mathbf{A_1}$	1.56188	1.83261	0.3375	0.59707
$\mathbf{A_2}$	2.55543	2.77462	1.42505	1.81042

about 1.18 (1.18), 2.85 (2.06) for $CuPN_2$, HPN_2 with GGA (LDA) approximation, respectively, indicating that HPN_2 is more anisotropic in shear compared to the others.

For a tetragonal system to be mechanically stable, the six anisotropic elastic constants must meet the Born stability criteria [40] given as follows:

$$\begin{cases} C_{11} > 0,\ C_{33} > 0, \quad C_{44} > 0, \quad C_{66} > 0,\ C_{11} > |C_{12}|, \\ C_{11}C_{33} > C_{13}^2 \\ (C_{11} + C_{12})C_{33} > 2C_{13}^2 \end{cases} \tag{14}$$

The values of the six elastic constants of the XPN_2 ($X = H, Cu$) chalcopyrite semiconductors, calculated at zero pressure, verify the conditions of mechanical stability (14), which indicate that they are mechanically stable in the tetragonal structure.

Yong modulus *E*, shear modulus *G*, bulk modulus *B*, Poisson ratio σ and the pair of elastic parameters can completely describe the elastic behavior of an isotropic system. However, the elastic constants C_{ij} must be evaluated first in order to compute the polycrystalline elastic parameters from first principle calculations and then transformed to macroscopic quantities by suitable averaging methods based on critical mechanics. The bulk modulus *B* representing the resistance to volume change and the shear modulus *G* representing the resistance to shear deformation. They can be obtained through a special averaging to the individual elastic constants C_{ij}. There are many different methods of such averaging. In this work, Voigt-Reuss-Hill averaging approximations have been studied [41–44] to evaluate *B* and *G*. For tetragonal lattice, the Voigt, Reuss, and Hill shear and bulk modulus B_V, B_R, B_H, G_V, G_R and G_H are given by the following expressions:

$$B_V = \frac{2C_{11} + 2C_{12} + 4C_{13} + C_{33}}{9} \tag{15}$$

$$B_R = \frac{(C_{11} + C_{12})C_{33} - 2C_{13}^2}{C_{11} + C_{12} - 4C_{13} + 2C_{33}} \tag{16}$$

$$G_V = \frac{4C_{11} + 2C_{33} - 4C_{13} - 2C_{12} + 12C_{44} + 6C_{66}}{30} \tag{17}$$

$$G_R = 15\left(\frac{4C_{11} + 4C_{12} + 8C_{13} + 2C_{33}}{(C_{11} + C_{12})C_{33} - 2C_{13}^2} + \frac{6}{C_{11} - C_{12}} + \frac{6}{C_{44}} + \frac{3}{C_{66}}\right)^{-1} \tag{18}$$

$$G_H = \frac{1}{2}(G_V + G_R) \ \text{ and } B_H = \frac{1}{2}(B_V + B_R) \tag{19}$$

The Young's modulus *E* and Poisson's ratio σ can be derived from *B* and *G* directly with the following relations

$$E = \frac{9BG}{(G + 3B)} \text{ and } \sigma = \frac{3B - 2G}{2(3B + G)} = \frac{1}{2}\left(1 - \frac{E}{3B}\right) \tag{20}$$

Table 6 presented the computed values of B_V, B_R, B_H, G_V, G_R, G_H,E_V,E_R, E_H, σ_V, σ_R, σ_H for $CuPN_2$ and HPN_2 using GGA and LDA.

The values bulk modulus obtained from the elastic constants through the Voigt-Reuss-Hill averaging method agree well with the values obtained from Birch-Murnaghan *EoS* fits. It ensures the accuracy and reliability of the used theoretical method and provides assurance in the proposed results for the elastic and electronic properties of $CuPN_2$ and HPN_2, presented in this work. The shear modulus value is lower that the bulk modulus value in all materials, therefore these materials are more resistive for compression than the shear. For pure covalent materials, the poison's ratio σ, has a small value $\sigma = 0.1$and has a typical value of $\sigma = 0.25$ for ionic materials. For solid characterized by metallic bonding, the typical σ value is 0.33. We have calculated the

Table 6. Modules of elasticity B_V, B_R, B_H, G_V, G_R, G_H,E_V,E_R, E_H, σ_V, σ_R, σ_H, A_B, A_G,A^U for $CuPN_2$and HPN_2 using GGA and LDA.

Compounds	$CuPN_2$		HPN_2	
Approximations	GGA	LDA	GGA	LDA
B_V	223.16	241.55	96.235	114.062
B_R	220.52	241.50	96.219	114.047
B_H	221.84	241.52	96.227	114.054
G_V	152.15	168.47	90.997	94.984
G_R	127.97	137.79	71.818	84.812
G_H	140.06	153.13	81.407	89.898
E_V	371.93	410.08	207.567	223.040
E_R	321.70	347.32	172.528	203.893
E_H	347.13	379.25	190.500	213.579
σ_V	0.22	0.21	0.14	0.174
σ_R	0.25	0.26	0.201	0.202
σ_H	0.23	0.23	0.17	0.187
$\frac{B_H}{G_H}$	1.58	1.57	1.18	1.26
A_B	0.5950	0.010	0.00831	0.00657
A_G	8.6320	10.0176	11.7796	5.65752
A^U	0.9567	1.1135	1.3354	0.5998

values of σ are about 0.23 for $CuPN_2$ and 0.17 (0.187) for HPN_2 with GGA (LDA). So, the Poisson ratio σ is less than 0.25, which point out that the forces are not completely central, or in other words the chemical bonds are characterized by an ionic-covalent mixture. These Poisson's ratio values suggest that the no-central forces contribution with certain amount affecting the considered tetragonal systems. The Yong's modulus for XPN_2 ($X = H, Cu$) chalcopyrite semiconductors are found to be between 213.65 and 379.25 GPa with LDA, corresponding to a rather medium stiffness in these compounds.

An important mechanical characteristic of solids is their brittle/ductile behavior which is closely associated to its fracture and reversible ability. Pugh's ratio B/G is one of the extensively used parameter to differentiate between brittle/ a ductile mechanical behavior of a solid [45]. Pugh proposed $B/G = 1.75$ (corresponds to $\sigma = 0.26$) as a criterion which separated ductile solids from brittle ones. If $B/G > 1.75$, the behavior of the material is ductile, otherwise it behaves like brittle. In the present study, it can be concluded that our compounds ($B/G < 1.75$) may be classified as brittle materials.

The elastic anisotropy is a key mechanical parameter to be determined because it estimate the distortion and micro-cracks in materials during their elaboration. The present work is comprised of three ways to estimate the elastic anisotropy in XPN_2 ($X = H, Cu$) chalcopyrite semiconductors. The first one is the calculation of the shear anisotropic factors. It provides a measure for determining the anisotropy degree in bonding between atoms in different planes. For tetragonal crystals the following parameters are used to express these relations [46]:

$$A_1 = 2C_{66}/(C_{11} - C_{12}) \text{ and } A_2 = 4C_{44}/(C_{11} + C_{33} - 2C_{13}) \quad (21)$$

The necessary condition of an isotropic material is that it should possess $A_1 = A_2 = 1$. Hence, the degree of elastic anisotropy linked with the deviation of A_1, A_2 from 1. We have observed that A_1 and A_2 are about to equal 1.83 and 2.77 (0.60 and 1.81), respectively, in $CuPN_2$ (HPN_2) using LDA approximation (see table 5). Therefore, according to these indexes, $CuPN_2$ and HPN_2 are characterized by noticeable shear anisotropy.

The calculation of the percentage of elastic anisotropy in compression (A_B) and in shear (A_G), defined as following [47]:

$$A_B = (B_V - B_R)/(B_V + B_R) \times 100 \text{ and } A_G = (G_V - G_R)/(G_V + G_R) \times 100,$$

where B and G are the bulk and the shear modulus, and the subscripts V and R indicate the Voigt and Reuss bounds. A_B and A_G are equal to zero in the case of an isotropic material. The deviation of A_B (A_G) from zero reveals the presence of an elastic anisotropy in compression (in shear). The largest possible anisotropy occurs when $A_B = A_G = 100\%$. The percentage of shear and bulk anisotropies in $CuPN_2$ (HPN_2) are found to be about 0.010% (0.00657%) and 10.0176% (5.65752%), respectively with LDA (see table 6). These results reveal that these materials, in bulk modulus, are characterized by a weak degree of anisotropy and in shear modulus, a noticeable anisotropy. It can be noticed that the $CuPN_2$ is more anisotropic than HPN_2.

Table 7. Longitudinal, transversal and average sound velocity (v_l, v_t, v_m in m/s) and Debye temperature (θ_D in K) for $CuPN_2$ and HPN_2 using GGA and LDA.

Compounds	Approximations	v_t	v_l	v_m	θ_D
$CuPN_2$	GGA	5237.71	8945.93	5807.58	803.538
	LDA	5383.47	9184.41	5968.57	835.312
HPN_2	GGA	5930.88	9205.27	6510.98	882.55
	LDA	6282.82	9532.82	6878.36	942.094

The third approach is to calculate the so-called universal index defined with the following relation [48]:

$$A^U = 5\frac{G_V}{G_R} + \frac{B_V}{B_R} - 6 \tag{22}$$

The A^U is equal to zero for an isotropic crystal. A value of A^U greater than zero sure the extent of crystal anisotropy. In our case A^U is about to equal 1.1135 and 0.5998 for $CuPN_2$ and HPN_2, respectively with LDA (see table 6). These results indicate that a noticeable elastic anisotropy is present in both compounds and $CuPN_2$ is more anisotropic than HPN_2.

At low temperature, vibratory excitations result solely from acoustic vibrations. Therefore, we can calculate the Debye temperature from the elastic constants rather than measure it from the low temperature specific heat. The temperature of Debye (θ_D) can be determined from the average sound velocity v_m by [49]:

$$\theta_D = \frac{h}{k_B}\left(\frac{3n}{4\pi}\left(\frac{N_a\ \rho}{M}\right)\right)^{\frac{1}{3}} v_m \tag{23}$$

Where h, k_B, N_a, ρ are the Planck's constant, Boltzmann's constant, Avogadro's number and density of the molecule, respectively. The molecular weight is M, and n is the number of atoms in the molecule. The average velocity v_m in polycrystalline materials is approximately given by: $v_m = \left(\frac{1}{3}\left(\frac{2}{v_t^3} + \frac{1}{v_l^3}\right)\right)^{-\frac{1}{3}}$ where v_l and v_t are longitudinal and transverse elastic velocities and can be obtained from the Navier equation:

$$v_l = \left(\frac{3B_H + 4G_H}{3\rho}\right)^{\frac{1}{2}} \text{ and } v_t = \left(\frac{G_H}{\rho}\right)^{\frac{1}{2}} \tag{24}$$

The values of ρ, v_l, v_t, v_m and θ_D are presented in table 7 calculated at zero pressure with *GGA* and *LDA* for XPN_2 ($X = H, Li, Na, Cu$). It appears from this table that elastic compression waves (longitudinal waves) propagate faster than elastic shear waves (transverse waves). There is no data is available in literature for the comparison with our results.

3.5. Transport properties

The calculation of transport properties such as electrical conductivity, electronic thermal conductivity and Seebeck coefficient are performed using BolzTrap, which is tool for evaluating those properties, by solving Boltzmann transport equation in the constant relaxation time approximation. The efficient thermoelectric materials of XPN_2 ($X = Cu, H$) compounds, have obvious attractive characteristics that makes them promising as thermoelectric energy converters in the range of medium temperature. The figure of merit of a thermoelectric compound is defined by $ZT = S^2\sigma T/\kappa$, where S, σ and κ are the Seebeck coefficient, the electrical conductivity and thermal conductivity, respectively. For the excellent thermoelectric materials, ZT is about or larger than unity [50]. The thermal and electrical conductivities and Seebeck coefficient are investigated first for the calculation of ZT. A potential difference is created by the temperature gradient among the two different materials in Seebeck effect. The movement of the free electrons is from higher to lower temperature portion. The unit of Seebeck coefficient is Volt per Kelvin [51].

The variation in Seebeck coefficient along with chemical potential (μ) for of the XPN_2 ($X = H, Cu$) chalcopyrite semiconductors at 300 (room temperature), 600, 900, 1200 K, is shown in figure 8.The values of μ_0 are 10 eV, 3.42 eV for $CuPN_2$ and HPN_2 respectively. The result has shown that the Seebeck coefficient with highest value at room temperature for the considered structures is achieved for $CuPN_2$ and HPN_2. For n-type of $CuPN_2$, HPN_2 compounds, Seebeck coefficients have the maximum values of 2832.56 $\mu V/K$ (at 300 K), 2676.85 $\mu V/K$ (at 300 K) respectively, which show that these compounds are good contestants for thermoelectrical materials.

Figure 8 shows that the graph of Seebeck coefficient increases with temperature at 300 K for $CuPN_2$ and HPN_2 materials then decreases almost exponentially with temperature. Conversely, it decreases almost exponentially with temperature for $CuPN_2$ and HPN_2 materials in n type.

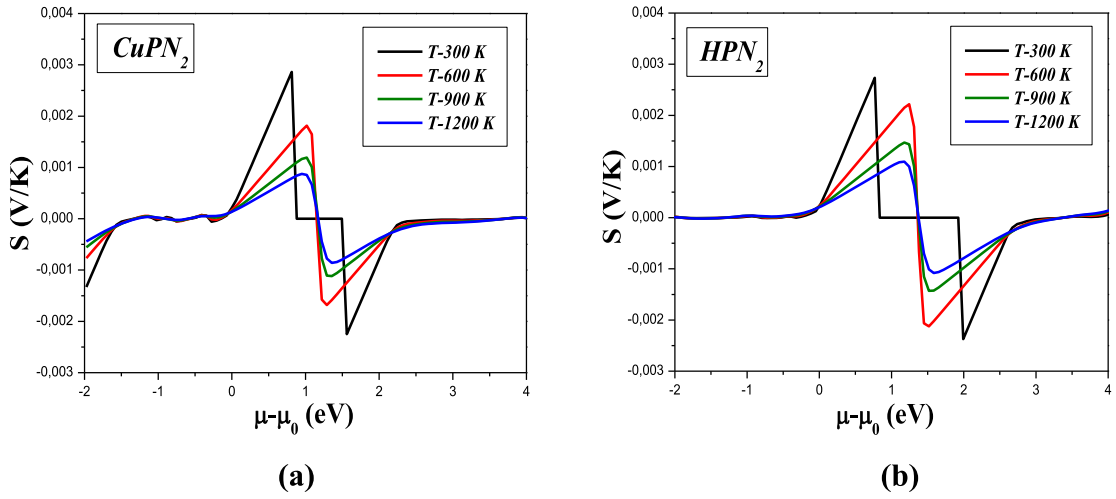

Figure 8. Seebeck coefficients for (a) $CuPN_2$, (b) HPN_2 as a function of chemical potential at 300, 600, 900 and 1200 K.

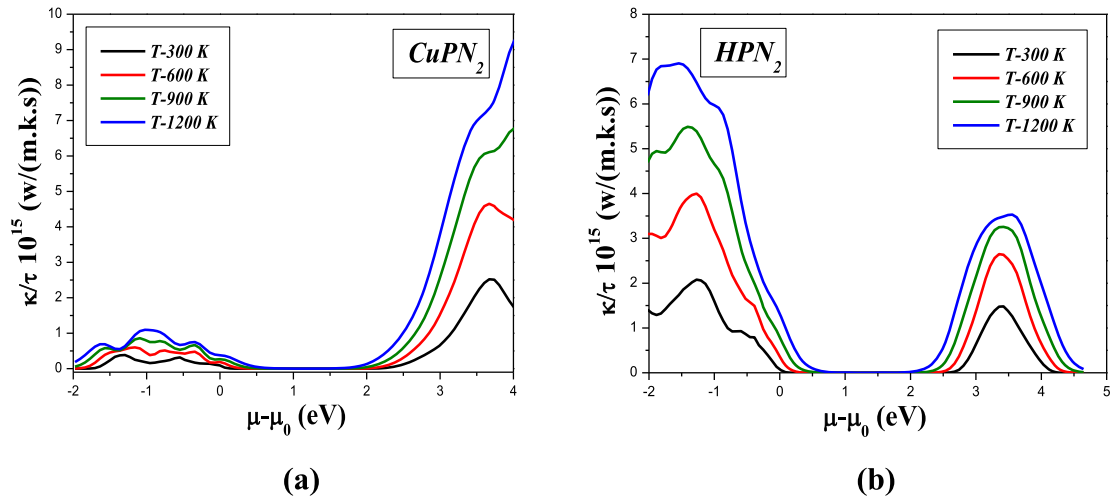

Figure 9. Electronic thermal conductivities for (a) $CuPN_2$, (b) HPN_2 as a function of chemical potential at 300, 600, 900 and 1200 K.

In this work, the electronic part of thermal conductivity, κ_{el} is obtained by assuming that it does not depends on the relaxation time τ and it is given by κ_{el}/τ. Small thermal conductivity is associated with good thermoelectric materials. Figure 9 present electronic thermal conductivities for $CuPN_2$ and HPN_2 compounds at 300 (room temperature), 600, 900, 1200 K. The electronic thermal conductivity for room temperature remains approximately zero between (0.17, 0.14) eV and (2.04, 2.45) eV chemical potential for $CuPN_2$ and HPN_2 compounds, respectively. The maximum efficiency is obtained in this region. Figure 9 shows a decrease in electronic thermal conductivity with temperature for p-type of XPN_2 ($X = Cu, H$) and then increases with temperature for n-type of XPN_2 ($X = Cu, H$). This property increases with temperature for XPN_2 ($X = Cu, H$) chalcopyrite semiconductors in n and p-types. Electrical conductivity is defined by the flow of free electrons in a compound. The movement of electrons from the high temperature regions to the low temperature regions is electric current [52]. High electrical conductivity is associated with efficient thermoelectric materials. The electrical conductivity for XPN_2 ($X = Cu, H$) chalcopyrite semiconductors are displayed in figure 10.

Figure 10 shows a decrease in electrical conductivity with temperature from 300 K to given temperatures for XPN_2 ($X = Cu, H$) chalcopyrite semiconductors then it is the same at other temperatures in n and p-type. Figures 11(a) and (b) display the figure of merit ZT for XPN_2 ($X = Cu, H$) chalcopyrite semiconductors. It shows that ZT for HPN_2 and $CuPN_2$ is very close to unity at room temperature for n and p-type. ZT sharply rises from zero to its peak value which suggests the use of these compounds in thermoelectric devices. From these results, it is concluded that there is a decrease in ZT value with temperature for all materials in n and p-type. The value of efficiency plotted in figure 11 also approves the reliability of the studied materials for thermoelectric

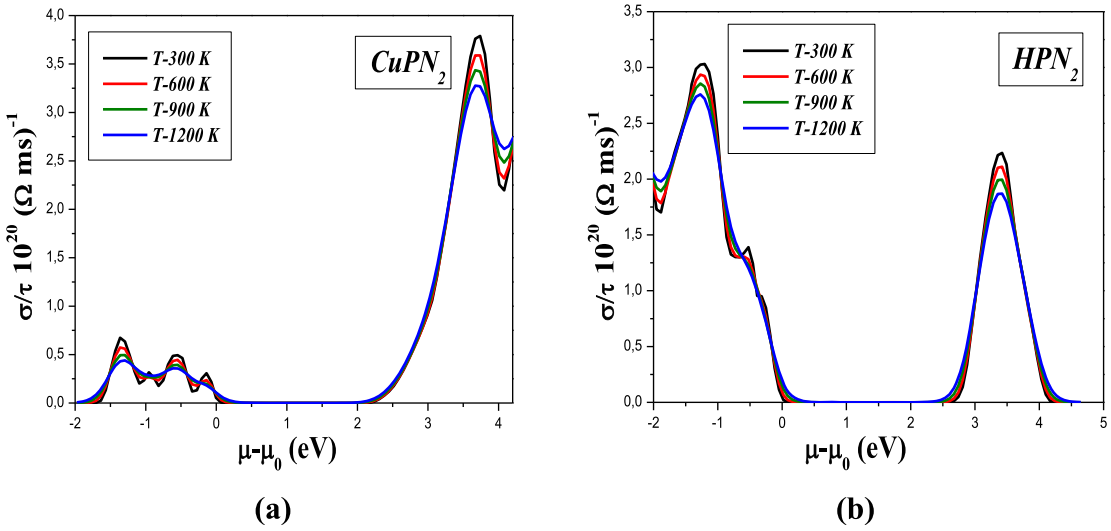

Figure 10. Electrical conductivities for (a) $CuPN_2$, (b) HPN_2 as a function of chemical potential at 300, 600, 900 and 1200 K.

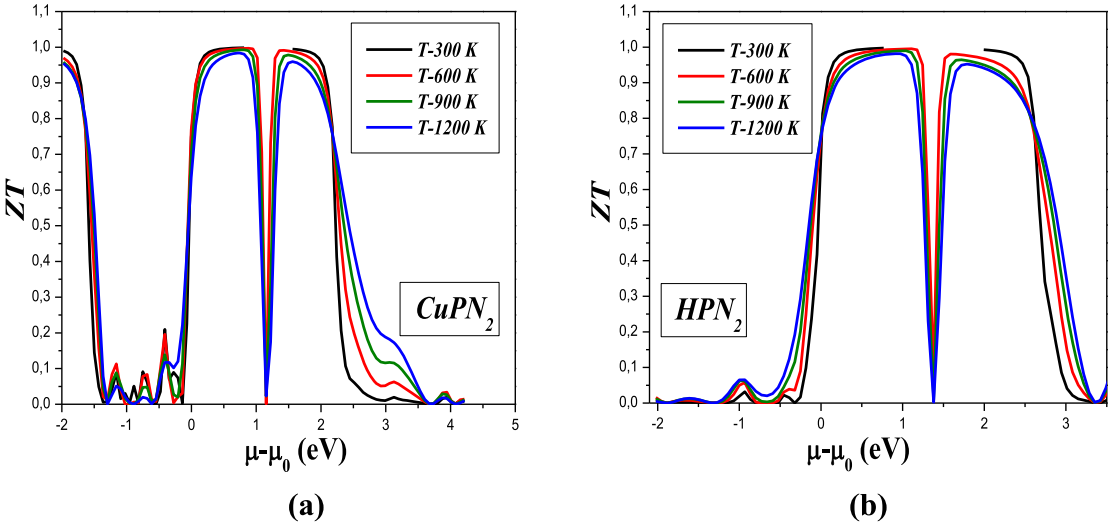

Figure 11. The figure of merit (ZT) for (a) $CuPN_2$, (b) HPN_2 as a function of chemical potential at 300, 600, 900 and 1200 K.

applications. Thus, the above studied materials can minimize the thermal losses and have the capability to fulfill the demands of energy specifically in high-temperature regions.

4. Conclusions

In this article, the structural parameters such as lattice constant, tetragonal ratio, anion displacement parameter for HPN_2 and $CuPN_2$ chalcopyrite semiconductors are calculated using GGA and LDA approximations. To compute electronic energy band gap, GGA, LDA, EV-GGA, mBJ-LDA and mBJ-GGA approximations are employed. The chalcopyrite structure is described by three parameters two lattice constants a and c, and internal parameter u, which define the position of anions in the base plane of unit cell (xy plane). The experimental and theoretical u values have interval (0.32–0.34), while the c/a ratio have interval (1.68–1.72) characterizing tetragonal distortion. Thus XPN_2 ($X = H, Cu$) compound can be revealed as a discrete group of extremely compressed chalcopyrite compounds. The structural parameters of XPN_2 ($X = H, Cu$) have substantial differences which are related to different size of the atoms. The theoretical data suggest that the replacement of H atoms with larger Cu atom decreases bond length very weakly between nitrogen atoms and these atoms by 0.95%; while the bond length of P-N increases by 2.38% (2.42%) occurs with GGA (LDA).

The gap between the conduction and valence bands calculated within mBJ-LDA approximation are 2.647 eV and 2.191 eV for HPN_2 and $CuPN_2$ respectively which gives HPN_2 and $CuPN_2$ the property to become a large band-gap semiconductor material. It has observed that the band dispersions in HPN_2 and $CuPN_2$ are very similar. The optical properties of HPN_2 and $CuPN_2$ have been also presented here. The general patterns of optical parameters such as real and imaginary part of dielectric constant, absorption coefficient and refractive index exhibit similar characteristics for both polarization *xx* (E⊥*c*-axis) and *zz* (E || *c*-axis), index has similar character for both polarizations, *xx* (E⊥*c*-axis), while they reveal small energy differences among them. The static dielectric constant $\varepsilon_1(0)$ and refractive index $n(0)$ increase from $CuPN_2$ to HPN_2. It is also observed that $CuPN_2$ and HPN_2 fall in the *UV* range and these materials can be good candidates for *UV* photo-detectors, *UV* light emitters and power electronic applications due to their fundamental absorption limits and the highest absorption peaks. A set of some macroscopic elastic moduli, including the bulk, Young's and shear moduli, Poisson's coefficient, average elastic wave velocities and Debye temperature, are calculated for chalcopyrite $CuPN_2$ and HPN_2 from the C_{ij} via the Voigt-Reuss-Hill approximations. In the last, the transport properties of $CuPN_2$ and HPN_2 are described by calculating the Seebeck coefficient, electronic thermal conductivity, electrical conductivity and figure of merit. The obtained maximum *ZT* value of considered structures for HPN_2 and $CuPN_2$ is very close to unity for *n* and *p*-type. The result related to transport properties suggests that these materials can be used in thermoelectric devices.

ORCID iDs

H Baaziz https://orcid.org/0000-0003-4860-2740

References

[1] Schnick W and Lucke J 1992 *Z. Anorg. Allg. Chem.* **610** 121
[2] Pucher F J, Hummel F and Schnick W 2015 *Eur. J. Inorg. Chem.* **2015** 1886–91
[3] Schnick W and Lücke J 1990 *Solid State Ion.* **38** 271
[4] Verma A S 2009 *Philos. Mag.* **89** 183
[5] Catella G C and Burlage D 1998 *Bull. Mater. Res. Soc.* **23** 28
[6] Zunger A and Jaffe J E 1983 *Phys. Rev. Lett.* **51** 662
[7] Lambrecht W R L and Rashkeev S N 2003 *J. Physics. Chem. Solids* **64** 1615
[8] Kazmerski L L 1983 *Nuovo Cimento* **D2** 2013
[9] Mishra S and Ganguli B 2011 *Solid State Commun.* **151** 523–8
[10] Mishra S and Ganguli B 2012 *J. Alloys Compd.* **512** 17–22
[11] Mishra S and Ganguli B 2015 *J. Solid State Chem.* **232** 131–7
[12] Parker D and Singh D J 2012 *Phys. Rev. B Condens. Matter Mater. Phys.* **85** 125209
[13] Reshak A H 2015 *J. Phys. Chem. Solids* **78** 46
[14] Schnick W 1993 *Angew. Chem., Int. Ed. Engl.* **32** 806
Schnick W 1993 *Angew. Chem. Int. Ed. Engl.* **105** 846
[15] Liu F, Carofalini S H, King-Smith R D and Vanderbilt D 1993 *Phys. Rev. Lett.* **70** 2750
[16] Gmelins Handbook of Inorganic Chemistry 1964 (Verlag Chemie: Weinheim) 8th Ed.vol. P.
[17] Dai H, Wong E W, Lu Y Z, Fan S and Liber C M 1995 *Nature* **375** 769
[18] Perdew J P and Wang Y 1992 *Phys. Rev. B* **45** 13244–9
[19] Perdew J P, Burke K and Ernzerhof M 1996 *Phys. Rev. Lett.* **77** 3865–8
[20] Engel E and Vosko S H 1993 *Phys. Rev. B* **47** 13164
[21] Becke A D and Johson E R 2006 *J. Chem. Phys.* **124** 221101
[22] Georg K, Madsen H and Singh D J 2006 *Comput. Phys. Commun.* **175** 67
[23] Blaha P, Schwarz K, Madsen G K H, Kvasnicka D and Luitz J (ed) *WIEN2K* ed K Schwarz (Austria: Vienna University of Technology) 2001
[24] Wang C S and Pickett W E 1983 *Phys. Rev. Lett.* **51** 597
[25] Jones R O and Gunnarsson O 1989 *Rev. Mod. Phys.* **61** 689
[26] Schnick W and Lücke J 1990 *Z. Anorg. Allg. Chem.* **19** 588
[27] Landskron K, Schmid S and Schnick W 2001 *Z. Anorg. Allg. Chem.* **627** 2469
[28] Shannon R D 1976 *Acta Cryst* A **32** 751–67
[29] O'Keeffe M and Hyde B G 1976 *Acta Crystallogr.* B **32** 2923
[30] Jaffe J E and Zunger A 1984 *Phys. Rev.* B **29** 1882
[31] Goryunova N A and Valov Y A (ed) 1974 *Sovetskoe Radio* (Moscow)
[32] Khan M A, Kashyap A, Solanki A K, Nautiyal T and Auluck S 1993 *Phys. Rev.* B **23** 16974
[33] Tributsch H 1977 *Z. Naturforsch.* A **32** 972
[34] Wooten F 1972 (New York and London: Academic press)
[35] Shan W, Walukiewicz W, Ager J W III, Haller E E, Geisz J F, Friedman D J, Olson J M and Kurtz S R 1999 *Phys. Rev. Lett.* **82** 1221
[36] Bakhshayeshi A, Sarmazdeh M M, Mendi R T and Boochani A 2017 *J. Electron. Mater.* **1** 2196–2204
[37] Penn D R 1962 *Phys. Rev.B* **128** 2093
[38] Khoshman J M, Jakkala P, Ingram D C and Kordesch M E 2016 *J. Non Cryst. Solids* **31** 440
[39] Ambrosch-Draxl C and Sofo J O 2006 *Comput. Phys. Commun.* **1** 175
[40] Grimvall G 1999 (Amsterdam: North-Holland)
[41] Reuss A and Angew Z 1929 *Math. Mech.* **9** 49

[42] Voigt W 1928 *Lehrbuch der Kristallphysik* doi:10.1007/978-3-663-15884-4
[43] Hill R 1952 *Proc. Phys. Soc. A* **65** 349
[44] Hill R 1963 *J. Mech. Phys. Solids* **11** 357
[45] Pugh S F 1954 *Philos. Mag.* **45** 823
[46] Al-Ghaferi A, Müllner P, Heinrich H, Kostorz G and Wiezorek J M K 2006 *Acta Mater.* **54** 881
[47] Ravindran P, Fast L, Korzhavyi P A and Johansson B 1998 *J. Appl. Phys.* **84** 4894
[48] Ranganathan S I and Ostoja-Starzewski M 2008 *Phys. Rev. Lett.* **101** 55504
[49] Anderson O L 1963 *J. Phys. Chem. Solids* **24** 909
[50] Rahnamaye Aliabad H A, Ghazanfari M, Ahmad I and Saeed M A 2012 *Comput. Mater. Sci.* **65** 509–19
[51] Bilal M, Khan B, Aliabad H A R, Maqbool M, Asadabadi S J and Ahmad I 2014 *Comput. Phys. Commun.* **185** 1394–8
[52] Rahnamaye Aliabad H A and Kheirabadi M 2014 *Physica B Condens. Matter.* **433** 157–64